JACS
JOURNAL OF THE AMERICAN CHEMICAL SOCIETY

ARTICLE

pubs.acs.org/JACS

Water-Medium and Solvent-Free Organic Reactions over a Bifunctional Catalyst with Au Nanoparticles Covalently Bonded to HS/SO_3H Functionalized Periodic Mesoporous Organosilica

Feng-Xia Zhu,[†] Wei Wang,[*,‡] and He-Xing Li[*,†]

[†]Department of Chemistry, Shanghai Normal University, Shanghai 200234, China

[‡]Department of Chemistry and Chemical Biology, University of New Mexico, Albuquerque, New Mexico 87131-0001, United States

Supporting Information

ABSTRACT: An operationally simple approach for the preparation of a new class of bifunctional Au nanoparticle−acid catalysts has been developed. In situ reduction of Au^{3+} with HS-functionalized periodic mesoporous organosilicas (PMOs) creates robust, fine Au nanoparticles and concomitantly produces a sulfonic acid moiety strongly bonded to PMOs. Characterizations of the nanostructures reveal that Au nanoparticles are formed with uniformed, narrow size distribution around 1−2 nm, which is very critical for essential catalytic activities. Moreover, the Au nanoparticles are mainly attached onto the pore surface rather than onto the outer surface with ordered mesoporous channels, allowing for maximal exposure to reaction substrates while minimizing Au nanoparticle leaching. Their higher S_{BET}, V_P, and D_P than either the Au-HS-PMO(Et) or the Au/SO_3H-PMO(Et) render the catalyst with comparably even higher catalytic efficiency than its homogeneous counterparts. Furthermore, the unique amphiphilic compartment of the Au-HS/SO_3H-PMO(Et) nanostructures enables organic reactions to proceed efficiently in a pure aqueous solution without using any organic solvents or even without water. As demonstrated experimentally, remarkably, the unique bifunctional Au-HS/SO_3H-PMO(Et) catalyst displays higher efficiencies in promoting water-medium alkyne hydration, intramolecular hydroamination, styrene oxidation, and three-component coupling reactions and even the solvent-free alkyne hydration process than its homogeneous catalysts. The robust catalyst can be easily recycled and used repetitively at least 10 times without loss of catalytic efficiency. These features render the catalyst particularly attractive in the practice of organic synthesis in an environmentally friendly manner.

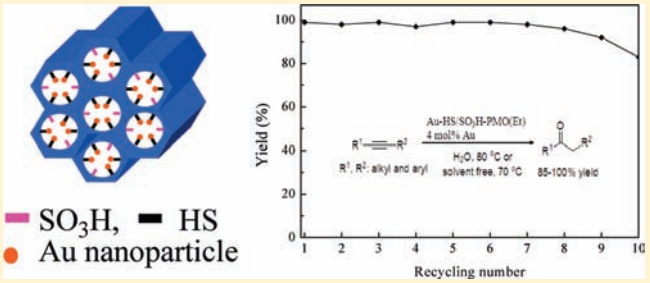

INTRODUCTION

One of the central goals in organic synthesis is to discover and identify reactions enabling processes to proceed in an environmentally friendly and sustainable way. Transition metals have enjoyed great success as the most widely catalytic systems in promoting organic reactions.[1] However, increasing concerns associated with toxicity, cost, and sustainability have prompted chemists to discover strategies to recover and reuse them. Moreover, pursuing organic reactions in a water medium is also an indispensible aim in contemporary organic synthesis because the use of water as a solvent has tremendous benefits including certainly obvious nontoxic, nonflammable, cheap, and widely available features.[2] While the merits of water are clear from a green chemistry perspective, the intrinsic limitations of performing organometallic-catalyzed reactions in water are also realized. One of the greatest limitations is the generation of an aqueous-based, metal-contaminated water stream and reduced catalytic efficiency.[3]

In the recent past, gold organometallic catalysts have been intensively explored in organic reactions with great success.[4] A typical example is the Au(I)-catalyzed alkyne hydration reactions, which have been the subject of intense investigations due to the broad utilities of the resulting carbonyl derivatives from the wide availability of alkynyl substrates.[5] This reaction is generally conducted in organic solvents, and in most cases, a Brønsted acid is required as a cocatalyst for effective transformation. Although they have high activity and selectivity, like other organometallic catalysts, homogeneous gold catalysts usually raise concerns of cost and environmental pollution; therefore, their recovery and reuse becomes essential in modern organic synthesis.

An important development in the field of gold catalysis is the discovery of gold nanoparticles with distinct catalytic properties in the past decade.[6] These Au nanoparticle catalysts are mainly employed in gas-phase oxidation reactions, and recently, they have also been expanded to liquid-phase organic reactions including cross-coupling[7] and oxidation reactions,[8] etc. Both the experimental findings and theoretical predictions demonstrate that Au particle size plays a crucial role in governing the catalytic activity, and the Au clusters must be smaller than 5 nm

Received: April 14, 2011
Published: June 27, 2011

for essentially high catalytic activity.[9] To date, several methods have been developed to prepare nanosized Au particles. However, the bare Au nanoparticles are difficultly separated from the reaction system and are also easily aggregated due to high surface energy.[10] To address these inherent limitations, significant efforts have been devoted to designing supported Au catalysts, but the control of Au particle size during reduction of Au ions and the stabilization of Au particles against leaching are quite a challenging and unmet goal.

Mesoporous silica supports allow for the high dispersion of metal nanoparticles owing to the ordered mesoporous pore channels and the high surface area. Functionalization with organic groups could enhance surface hydrophobility, which may facilitate the adsorption of organic molecules, especially in aqueous medium. Nevertheless, the organic groups terminally bonded to the pore surface might block the pore channel and even damage the ordered mesoporous structure. Periodic mesoporous organosilica (PMO) with organic fragments embedded in silica walls could greatly overcome these problems.[11] More importantly, the chemical and physical properties of PMO can be easily tuned by changing the organic functionalities inside the framework, which may offer diversified opportunities for their applications. Recently, Vinu et al. reported the Au nanoparticles immobilized onto a mesoporous carbon nitride support, which could control the Au particle size by the pore channel diameter.[12] However, the direct reduction of Au^{3+} by KBH_4 alkaline solution resulted in relatively large Au nanoparticles with average size around 7 nm, which were unfavorable for catalysis and also easily leached off from the support.

In this account, we wish to report an alternative operationally simple approach to preparing a novel supported Au catalyst by in situ reduction of Au^{3+} with HS (HS = $HS-CH_2-CH_2-CH_2$ group) incorporated into the ethyl (Et)-bridged PMO. This design strategy kills three birds with one stone: (1) forming very tiny Au nanoparticles with average size around 1−2 nm; (2) stabilizing the Au nanoparticles against aggregation and/or leaching via coordination with the unreacted HS ligand; and (3) oxidizing HS to produce SO_3H as a Brønsted acid covalently bonded to the PMO(Et) support. As a result, notably, the as-prepared Au-HS/SO_3H-PMO(Et) acts as a bifunctional catalyst in solvent-free and water-medium hydration of alkynes and intramolecular hydroamination, styrene oxidation, and three-component coupling reactions with high efficiency. More importantly, it can be easily recycled and used repetitively for more than 10 times without loss of catalytic efficiency.

RESULTS AND DISCUSSION

1. Preparation of Bifunctional Covalently Bonded Au Nanoparticles and HS/SO_3H Periodic Mesoporous Organosilicas and Structural Characterizations. *Preparation.* Scheme 1 briefly illustrated preparation of Au-HS/SO_3H-PMO(Et). First, the HS-PMO(Et) with HS/Si and Et/Si molar ratios of 5.0% and 47% was prepared by P123 surfactant-directed co-condensation between (3-mercaptopropyl) trimethoxysilane (MPTMS) and bis(triethoxysilyl)ethane (BTEE). Then, the HS-PMO(Et) was added into $HAuCl_4$ ethanol solution and kept stirring at room temperature for 24 h. This initiated three sequential processes: reduction of Au^{3+} to Au nanoparticles, oxidation of HS to SO_3H, and coordination of the Au nanoparticles with the unreacted HS ligand. For comparison, the Au-HS/SO_3H-SBA-15 was also synthesized by in situ reduction of $HAuCl_4$ with the HS-SBA-15 prepared by P123

Scheme 1. Illustration of the Preparation of the Au-SH/SO_3H-PMO(Et)[a]

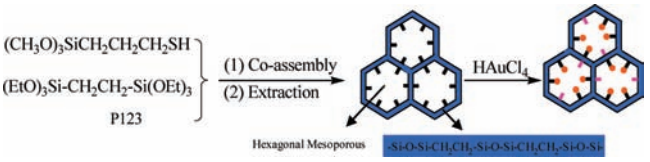

[a] Pink box = SO_3H, black box = SH, orange circle = Au.

surfactant-directed co-condensation between (3-mercaptopropyl) trimethoxysilane and tetraethoxysilane. Meanwhile, the Au/HS-PMO(Et) catalyst was also prepared by direct depositing Au nanoparticles onto the HS-PMO(Et) support. The bare Au nanoparticles with average size around 3 nm were prepared by reduction of Au^{3+} with *tert*-butylamine-borane in oleylamine/tetralin solution. Finally, the Au/SO_3H-PMO(Et) catalyst was synthesized by depositing Au nanoparticles onto the SO_3H-PMO(Et) obtained by oxidizing the HS-PMO(Et) with H_2O_2 (see the Experimental Section for details).

Structure Characterizations. As shown in Figure 1, the XPS spectra revealed that all the Au species in the Au-HS/SO_3H-PMO(Et) were present in the metallic state, corresponding to the binding energy (BE) of 84.7 eV in the $Au_{4f7/2}$ level,[13] which could be further confirmed by reduction with $NaBH_4$ solution (Figure S1, Supporting Information). The S species were present in −2 and +6 oxidation states, corresponding to HS and SO_3H groups with the BE around 164.4 and 168.8 eV in the S_{2p} level, respectively. According to the calculation from peak areas, the HS/SO_3H molar ratio was determined as 15:1, suggesting only a little portion of HS was oxidized into SO_3H. The Au BE in Au-HS/SO_3H-PMO(Et) shifted negatively by 0.3 eV compared to that of the bare Au nanoparticles. Meanwhile, the S BE in the HS groups in the Au-HS/SO_3H-PMO(Et) shifted positively by 0.4 eV compared to that in HS-PMO(Et). These results clearly demonstrated the in situ reduction of $HAuCl_4$ by HS groups to produce Au nanoparticles and SO_3H groups, followed by coordinating the Au nanoparticles with the unreacted HS-ligands, in which the S donated partial electrons to Au through d−p feedback, making the Au electron enriched and the S electron deficient. No significant S BE shift in the SO_3H groups in the Au-HS/SO_3H-PMO(Et) was found in comparison with that in the SO_3H-PMO(Et), implying no coordination bonding formed between SO_3H and Au nanoparticles. The Au-HS/SO_3H-SBA-15 displayed XPS spectra similar to the Au-HS/SO_3H-PMO(Et). However, no significant BE shift of either Au or S was observed in the Au/HS-PMO(Et) sample (see the XPS spectra in Figure S2, Supporting Information), indicating the absence of coordination between the Au and HS-ligand, possibly due to the large Au particle size.

The TG/DTA analysis (Figure S3, Supporting Information) demonstrated the complete removal of surfactant template since no significant signal around 250 °C indicative of P123 was observed.[14] Besides an endothermic peak around 80 °C with weight loss of about 3% due to the desorption of physisorbed water, solvent, or other organic residues, the Au-HS/SO_3H-PMO(Et) displayed three exothermic peaks at 340, 425, and 631 °C with total weight loss around 23%, corresponding to the combustion of $HS-CH_2-CH_2-CH_2$ and $SO_3H-CH_2-CH_2-CH_2$ groups covalently bonded to the PMO(Et) and the ethyl groups

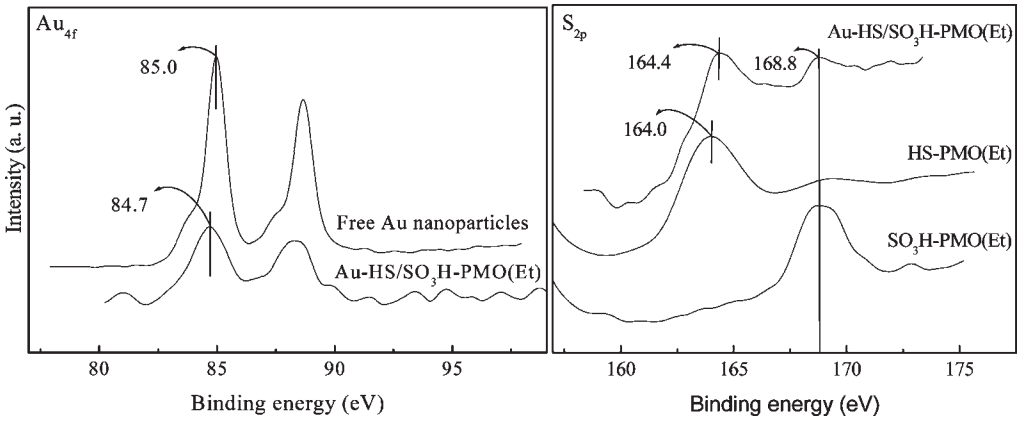

Figure 1. XPS spectra of different samples at Au_{4f} and S_{2p} levels.

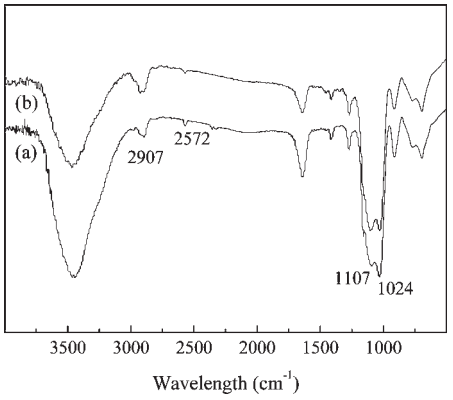

Figure 2. FT-IR spectra of (a) HS-PMO(Et) and (b) Au-HS/SO_3H-PMO(Et).

embedded in the silica walls. The FT-IR spectra of HS-PMO(Et) and Au-HS/SO_3H-PMO(Et) (Figure 2) displayed absorbance peaks around 2907 cm^{-1} indicative of the stretch vibration of the C−H bond in either the HS−CH_2−CH_2−CH_2− group or the −CH_2−CH_2− group. Meanwhile, the absorbance bands at 1024 and 1107 cm^{-1} could be assigned to the ν_{Si-O} and ν_{Si-C} vibrations, respectively.[15] The weak absorbance band at 2572 cm^{-1} could be attributed to the vibration of the HS group.[16] In comparison with the HS-PMO(Et), the Au-HS/SO_3H-PMO(Et) displayed a much weaker peak due to the oxidation of partial HS groups to the SO_3H groups and/or the coordination of the HS-ligand with the Au nanoparticles.

The presence of SH, SO_3H, and Et groups in the Au-HS/SO_3H-PMO(Et) could be further confirmed by solid NMR spectra. As shown in Figure 3, the ^{29}Si CP-MAS NMR spectrum display two peaks downfield corresponding to T^3 ($\delta = -66$ ppm) and T^2 ($\delta = -59$ ppm), where $T^m = RSi(OSi)_m(OH)_{3-m}$ ($m = 1\sim3$). The absence of Q^n peaks ($Q^n = Si(OSi)_n(OH)_{4-n}$, $n = 2\sim4$) suggested that all Si species were covalently bonded with C atoms.[17] According to the ^{13}C CP-MAS NMR spectrum, the Au-HS/SO_3H-PMO(Et) displayed a strong peak around 2.7 ppm indicative of the C atoms in the ethyl group in the framework.[18] The other three peaks around 9, 15, and 55 ppm could be assigned to three carbon atoms in the $HO_3S-CH_2-CH_2-CH_2$ group.[19] A weak peak around 25 ppm could be attributed to the C atom connecting with the S in the HS−CH_2−CH_2−CH_2 group.[20]

The above XPS, TG/DTA, FT-IR, and NMR characterizations demonstrated the presence of both HS−CH_2−CH_2−CH_2 and $HO_3S-CH_2-CH_2-CH_2$ groups in the Au-HS/SO_3H-PMO(Et) catalyst. To determine the location positions of these HS and SO_3H functional groups, two kinds of HS-PMO(Et) samples with HS content of 5% were prepared via different methods (see Scheme S1, Supporting Information). The HS-PMO(Et)-A was prepared according to the method used in the present work (Method A), but the P123 template was not extracted. The HS-PMO(Et)-B was prepared using Method B, as follows. First, the PMO(Et) containing the P123 template was synthesized by coassembly of P123 and bis(triethoxysilyl)ethane. Then, the HS-PMO(Et)-B was obtained by grafting (3-mercaptopropyl) trimethoxysilane onto the above PMO(Et). Since the mesoporous channels in the PMO(Et) were occupied by P123 template molecules, the HS groups in the HS-PMO(Et)-B were mainly positioned on the outer surface. The content of HS groups in either HS-PMO(Et)-A or HS-PMO(Et)-B samples was then determined by Pt^{2+} adsorption.[16a,21] Since the mesoporous channels were occupied by P123 template molecules, only the HS groups on the outer surface could coordinate with the Pt^{2+}. In each run of experiments, 50 mg of sample was added into 10 mL of an aqueous solution containing 50 ppm of Pt^{2+}. After being stirred for 2 h at room temperature, the Pt^{2+} content left in the solution was measured by ICP analysis. In the presence of HS-PMO(Et)-A, the Pt^{2+} content in the solution decreased by only 1.0 ppm, while in the presence of HS-PMO(Et)-B, the Pt^{2+} content decreased by 9.5 ppm. These results clearly demonstrated that most of the HS groups in the as-prepared Au-SH/SO_3H-PMO(Et) were located on the pore surface rather than the outer surface of PMO(Et). Accordingly, the SO_3H groups were also mainly planted onto the pore surface of PMO(Et), taking into account that the SO_3H groups were generated from the oxidation of HS groups.

As shown in Figure 4, both the Au-HS/SO_3H-PMO(Et) and the HS-PMO(Et) displayed typical IV type N_2 adsorption−desorption isotherms with an H_1-type hysteresis loop indicative of the mesoporous structure.[22] The low-angle XRD patterns demonstrated that these two samples were comprised of ordered 2D *P6mm* hexagonal mesoporous channels.[23] In comparison with the HS-PMO(Et), the Au-HS/SO_3H-PMO(Et) showed a positive shift in peak position, corresponding to the enhanced wall thickness, which suggested that the Au nanoparticles were mainly fixed onto the pore surface rather than onto the outer

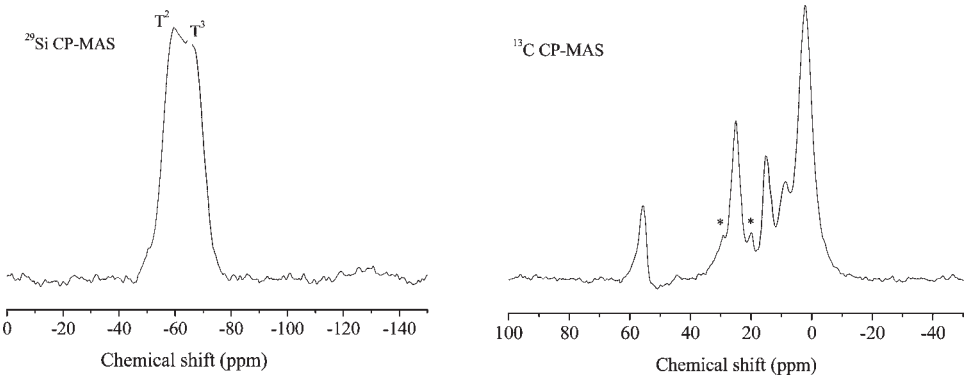

Figure 3. Solid ^{29}Si and ^{13}C NMR spectra of the Au-HS/SO_3H-PMO(Et).

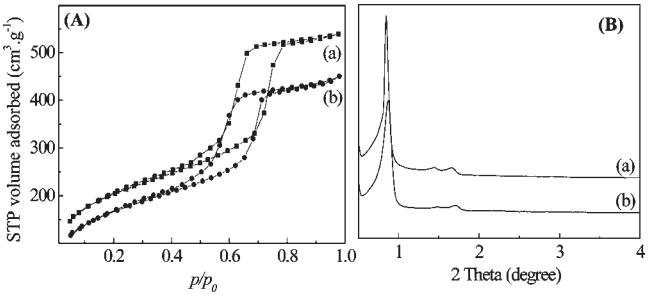

Figure 4. (A) N_2 adsorption−desorption isotherms and (B) low-angle XRD patterns of (a) HS-PMO(Et) and (b) Au-HS/SO_3H-PMO(Et).

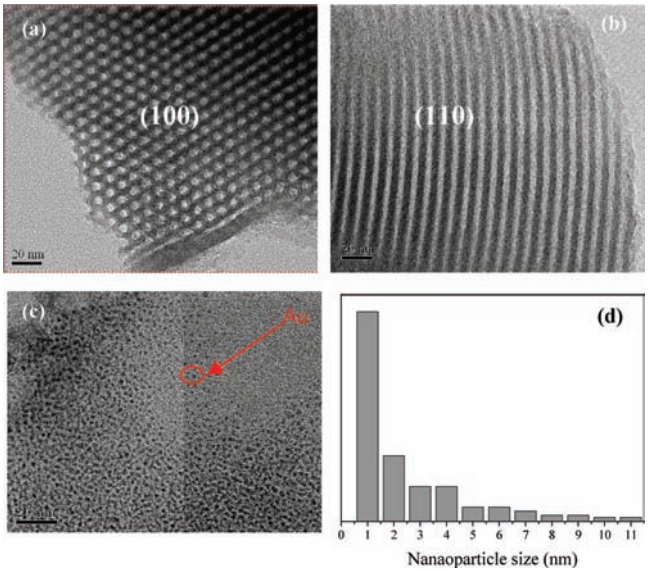

Figure 5. (a and b) HRTEM images of Au-HS/SO_3H-PMO(Et) and (c) the HRTEM image of Au-HS/SO_3H-PMO(Et) dissolved in HF solution. (d) The corresponding Au particle size distribution diagram.

surface, in good accordance with the location positions of HS and SO_3H functional groups.

The HRTEM images in Figure 5 clearly showed the ordered mesoporous channels in the Au-HS/SO_3H-PMO(Et) catalyst. Although the XPS analysis verified the presence of metallic Au, no significant Au particles were observed due to the uniform dispersion and extremely tiny Au particle size, which was consistent with

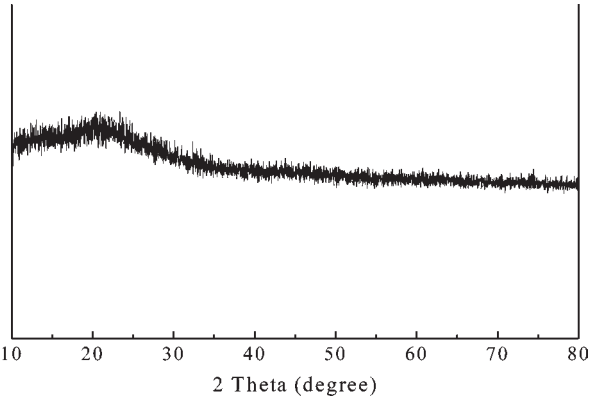

Figure 6. Wide-angle XRD pattern of the Au-HS/SO_3H-PMO(Et).

the wide-angle XRD pattern (Figure 6) since no significant diffractional peaks indicative of the metallic Au phase were observed. Meanwhile, the UV−vis DRS spectrum (Figure S4, Supporting Information) displayed a broad light absorbance band centered at 508 nm, corresponding to the plasma effect, which further confirmed the presence of tiny Au nanoparticles with average size less than 5 nm. To observe the Au particles, the Au-HS/SO_3H-PMO(Et) was etched in HF solution to remove the support. As shown in Figure 5, the HRTEM clearly displayed uniform Au nanoparticles with narrow size distribution around 1−2 nm. Meanwhile, the CO chemisorption and the EXAFS were also employed to estimate the Au particle size. On one hand, the Au active surface area (S_{act}) of the Au-SH/SO_3H-PMO(Et) catalyst was determined as 185 m^2/g by CO chemisorption, from which the average Au particle size was calculated as 1.6 nm according to the following equation.[24]

$$d = 6000/(\rho \times S_{act})$$

where ρ refers to the density of Au metal (19.3 g/cm^3). On the other hand, the Au L_3-edge XANES spectra (Figure 7) revealed that the Au-SH/SO_3H-PMO(Et) displayed a broadened peak at 11.95 keV in comparison with the Au foil, implying the tiny Au particles.[25] The Au coordination number, Au−Au bonding distance, and S/Au atomic ratio in the Au-SH/SO_3H-PMO(Et) were calculated as 3.5, 0.281 nm, and 2.6, respectively, while the Au foil displayed a Au coordination number of 12 and a Au−Au bonding distance of 0.287 nm. The shorter Au−Au bonding distance implied a smaller Au particle size. According to the correlation of the Au−Au bonding distance and Au particle size,[26] the Au

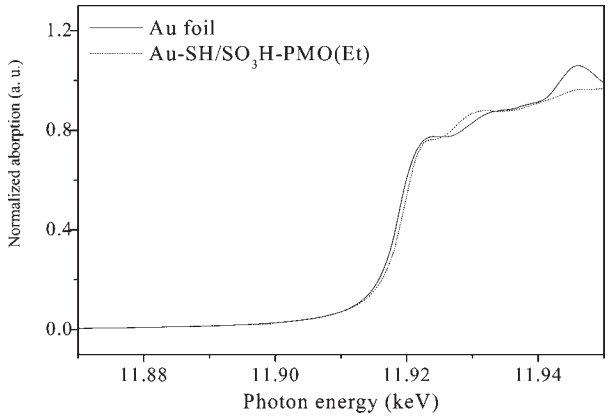

Figure 7. Au L_3-edge XANES spectra of the Au foil and the Au-SH/SO_3H-PMO(Et) catalyst.

particle size in the Au-SH/SO_3H-PMO(Et) catalyst was roughly estimated as 1.2 nm. The Au particle size estimated from either the CO chemisorption or the EXAFS was consistent with that observed from the HRTEM image. The TEM images (Figure S5, Supporting Information) demonstrated that the Au-HS/SO_3H-SBA-15 displayed slightly bigger Au particle size than the Au-HS/SO_3H-PMO(Et), suggesting that the presence of Et groups in the silica support could prevent the aggregation of Au nanoparticles owing to the enhanced surface hydrophobicity. Moreover, the Au-HS/SO_3H-PMO(Et) exhibited much smaller Au particles than either the bare Au nanoparticles obtained by direct reduction of $HAuCl_4$ with *tert*-butylamine-borane or the Au/HS-PMO(Et) obtained by depositing the Au nanoparticles onto the HS-PMO(Et) (also see Figure S5, Supporting Information), obviously owing to the in situ reduction of $HAuCl_4$ and coordination of Au nanoparticles with the HS-ligand, which effectively inhibited the particle aggregation.

Other structural parameters are summarized in Table 1. The Au-HS/SO_3H-PMO(Et) exhibited lower surface area (S_{BET}), pore volume (V_P), and pore diameter (D_P) than the HS-PMO(Et) due to the occupation of Au nanoparticles in pore channels. Nevertheless, it displayed higher S_{BET}, V_P, and D_P than the Au-HS/SO_3H-SBA-15 owing to the incorporation of Et groups into the silica walls, which might enlarge the pore channels. Furthermore, it showed higher S_{BET}, V_P, and D_P than either the Au-HS-PMO(Et) or the Au/SO_3H-PMO(Et), obviously owing to the smaller size of Au nanoparticles inside the mesopore channels.

Catalytic Performances. The catalytic performances were mainly examined in solvent-free and water-medium alkyne hydration reactions. Table 1 summarized the catalytic performances of different catalysts in water-medium phenylacetylene hydration. Besides the acetophenone, no other products were identified, suggesting all these catalysts were exclusively selective. Both HS-PMO(Et) and SO_3H-PMO(Et) were inactive, implying that the Au active sites were essential for the present reactions. Interestingly, the Au/HS-PMO(Et) was inactive, but the Au/SO_3H-PMO(Et) could catalyze the alkyne hydration in the absence of H_2SO_4 in aqueous solution. However, when trace H_2SO_4 was added into the reaction system, the Au/HS-PMO(Et) displayed slightly higher activity than the Au/SO_3H-PMO(Et). These results clearly demonstrated that the alkyne hydration should be cocatalyzed by the metallic Au and the Brønsted acid synergistically. Therefore, the Au-HS/SO_3H-PMO(Et) acted as a bifunctional catalyst resulting from both the Au nanoparticles and the SO_3H groups covalently bonded to the PMO(Et) support. Importantly, the distance between the Au-deposited site and the SO_3H acid site plays a key role in governing their cooperative effect. The average distance between the SO_3H acid site and Au deposited site can be controlled by varying the content of SH functional groups in the Au-HS/SO_3H-PMO(Et) catalyst, taking into account that the SO_3H was generated from the oxidation of SH. With the fixed Au loading, the average distance decreased gradually with the increase of the HS content. Therefore, besides Au-HS/SO_3H-PMO(Et) with HS content of 5%, Au-HS/SO_3H-PMO(Et)-1 and the Au-HS/SO_3H-PMO(Et)-2 with respective HS content of 3% and 10% were synthesized for comparison, and their catalytic performances were examined. As shown in Table 1, the activity first increased and then decreased with the increase of the HS content. The Au-HS/SO_3H-PMO(Et)-1

Table 1. Structural Parameters and Catalytic Efficiencies in Water-Medium Phenylacetylene Hydration[a]

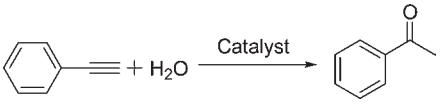

sample	loading (mmol/g)	SH/SO_3H molar ratio	S_{BET} (m^2/g)	V_P (cm^3/g)	D_P (nm)	H_2SO_4 (mmol)	yield (%)
HS-PMO(Et)	0	/	712	0.64	8.0	0	0
SO_3H-PMO(Et)	0	0	699	0.63	7.8	0	0
Au-HS/SO_3H-PMO(Et)-1[b]	0.10	4:3	683	0.59	7.5	0	87
Au-HS/SO_3H-PMO(Et)[b]	0.10	15:1	591	0.55	7.2	0	99
Au-HS/SO_3H-PMO(Et)-2[b]	0.10	31:1	505	0.47	6.8	0	93
Au-HS/SO_3H-SBA-15	0.096	/	475	0.43	7.0	0	90
Au/SO_3H-PMO(Et)	0.10	0	486	0.47	6.5	0	29
Au/HS-PMO(Et)	0.12	/	472	0.58	6.5	0	0
Au/HS-PMO(Et)	0.12	/	472	0.58	6.5	0.25	36
Au(PPh_3)Cl[c]	/	/	/	/	/	0.25	24
Au-HS/SO_3H-PMO(Et)[d]	0.096		455	0.41	6.4	0	83

[a] Unless specified, see reaction conditions in the Experimental Section. [b] The Au-HS/SO_3HPMO(Et)-1, Au-HS/SO_3H-PMO(Et), and Au-HS/SO_3H-PMO(Et)-2 catalysts were prepared from the HS-PMO(Et) with the original HS-content of 3%, 5%, and 10%, respectively. [c] Reaction temperature = 100 °C, reaction time = 7 h. [d] After being reused 10 times.

dx.doi.org/10.1021/ja203450g |*J. Am. Chem. Soc.* 2011, 133, 11632–11640

with low HS content (3%) exhibited poorer activity, possibly due to the relatively longer distance between the acid site and the Au-deposited site, which might reduce their synergetic effect. Although the Au-HS/SO_3H-PMO(Et)-2 with high HS content (10%) displayed relatively shorter distance between the acid site and the Au-deposited site, it also showed lower activity which could mainly be attributed to partial blockage of mesopore channels and damage of ordered mesoporous structures, corresponding to the abrupt decrease in surface area (S_{BET}), pore volume (V_P), and pore diameter (D_P). The Au-HS/SO_3H-PMO(Et) with HS-content of 5% was thus determined as an optimum catalyst. With the similar Au loading, the Au-HS/SO_3H-PMO(Et) had higher activity than the Au-HS/SO_3H-SBA-15, possibly owing to the small Au nanoparticle size, high surface area, large pore channels, and enhanced surface hydrophobility resulting from the ethyl functionalization, which facilitated the diffusion and adsorption of organic reactants.[27] The higher activity of the Au-HS/SO_3H-PMO(Et) than that of the Au/SO_3H-PMO(Et) could be attributed to the smaller Au particle size. Meanwhile, the Au nanoparticles were stabilized by coordination with the HS ligand, which effectively inhibited their leaching off during catalysis.

To demonstrate the generality of the bifunctional Au-HS/SO_3H-PMO(Et)-catalyzed alkyne hydration reactions, we probed different substrates with significant structural variation (Table 2). Table 2 further demonstrated that the Au-HS/SO_3H-PMO(Et) exhibited high activity either in water-medium or even in solvent-free alkyne hydration under mild reaction conditions. The presence of substitutes on the *p*-position of benzene had very little influence on the catalytic efficiencies (entries 1−5). However, slightly lower yields (93% and 85%) and longer reaction times (3 and 4 h, respectively) for more steric o-substituted substrates were observed (entries 6 and 7), implying that the steric hindrance played a certain role in the reaction efficiency. The process was also applicable to aliphatic alkynes in excellent yields (96−97%, entries 8 and 9). Symmetrical internal alkynes were also proved to be effective substrates for the hydration processes (entries 10 and 11). Importantly, when an unsymmetrical internal alkyne engaged in the reaction, one exclusive regioisomer was obtained in very high yield (95%, entry 12). Excellent yields were also achieved in solvent-free alkyne hydration even at relatively lower temperature (70 °C). On one hand, this may be attributed to the unique amphiphilic nanostructures with high surface areas which could efficiently adsorb moisture (as the water source) and hydrophobic organic reactants onto the catalyst. On the other hand, the water molecules coordinated with the acidic sites of the silica surface were sufficiently nucleophilic to react with the electrophilic species involved in the reaction.

To further demonstrate the utility of the unique Au-HS/SO_3H-PMO(Et) catalyst, we also tested the water-medium intramolecular hydroamination,[28] styrene oxidation[29] (Table 3), and even three-component A^3-coupling[30] (Table 4) reactions. To our surprise, the Au-HS/SO_3H-PMO(Et) exhibited much higher activity than the Au(PPh_3)Cl homogeneous catalyst in these reactions (Table 3), showing that the Au nanoparticles were extremely active owing to the unique quantum size effect and cooperative effects between the

Table 2. Solvent-Free and Water-Medium Alkyne Hydrations Over the Au-HS/SO_3H-PMO(Et) Catalyst[a]

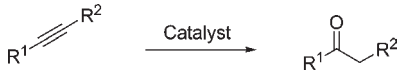

entry	R^1	R^2	H_2O (mL)	T (°C)	t (h)	yield (%)
1	Ph	H	4.0	80	1.5	99
2	4-MeOPh	H	4.0	80	1.5	98
3	4-CF_3Ph	H	4.0	80	1.5	84
4	4-MePh	H	4.0	80	1.5	94
5	4-BrPh	H	4.0	80	1.5	96
6	2-MePh	H	4.0	80	3.0	93
7	2-CF_3Ph	H	4.0	80	4.0	85
8	*n*-C_6H_{13}	H	4.0	80	1.5	97
9	*n*-C_8H_{17}	H	4.0	80	1.5	95
10	Ph	Ph	4.0	80	4.0	88
11	*n*-Pr	*n*-Pr	4.0	80	1.5	94
12	Ph	CH_3	4.0	80	1.5	95
13	Ph	H	0	70	1.5	100
14	4-MeOPh	H	0	70	1.5	100
15	4-CF_3Ph	H	0	70	1.5	94

[a] Unless specified, see reaction conditions in Experimental Section.

Table 3. Catalytic Efficiencies in Water-Medium Intramolecular Hydroamination and Styrene Oxidation Reactions[a]

Catalyst	Reaction	Conv. (%)	Yield (%)
Au-HS/SO_3H-PMO(Et)	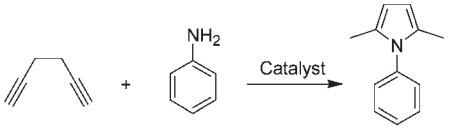	87	87
Au(PPh_3)Cl		23 (37)[b]	23 (35)[b]
Au-HS/SO_3H-PMO(Et)	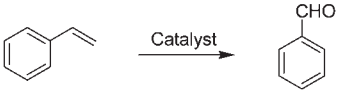	35	29
Au(PPh_3)Cl		21 (33)[b]	17 (24)[b]

[a] Unless specified, see reaction conditions in Experimental Section. [b] The values in the parentheses were obtained on the Au(PPh_3)Cl catalyst in the presence of 0.25 mmol of H_2SO_4.

Table 4. Catalytic Efficiencies in Water-Medium "One-Pot" A^3-Coupling Reactions[a]

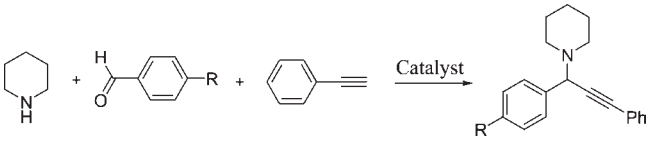

catalyst	R	conv. (%)	yield (%)
Au-HS/SO_3H-PMO(Et)	H	98	98
Au-HS/SO_3H-PMO(Et)	CH_3	81	81
Au-HS/SO_3H-PMO(Et)	Cl	>99	>99
Au(PPh_3)Cl	H	12 (20)[b]	12 (21)[b]

[a] Unless specified, see reaction conditions in Experimental Section. [b] The values in the parentheses were obtained on the Au(PPh_3)Cl catalyst in the presence of 0.25 mmol of H_2SO_4.

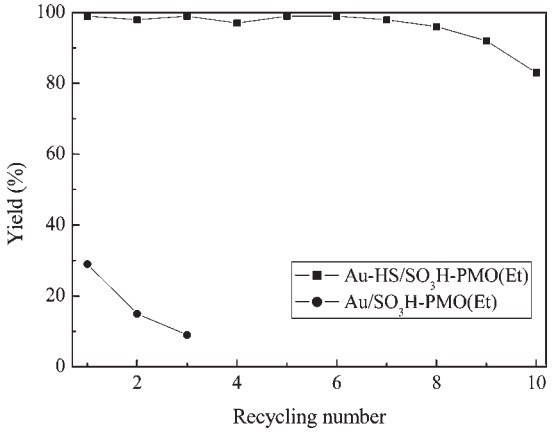

Figure 8. Recycling test of the Au-SH/SO_3H-PMO(Et) and Au/SO_3H-PMO(Et) catalysts in water-medium hydration of phenylacetylene. Reaction conditions are given in Table 1.

Au active phase and the SO_3H acid active site. The acid effect on the Au catalytic efficiency could be confirmed by the fact that addition of a catalytic amount of H_2SO_4 could enhance the catalytic activity of Au(PPh_3)Cl in homogeneous systems (see the values in the parentheses in Tables 3 and 4). Nevertheless, the cooperative effect between the Au active phase and the acid active site is more pronounced due to the proximity in the reaction compartments.

Moreover, the Au-HS/SO_3H-PMO(Et) displayed much higher activity in water-medium A^3-coupling reactions than the corresponding Au(PPh_3)Cl homogeneous catalyst (Table 4).[30] The presence of the CH_3 substitute on the benzaldehyde greatly decreased the catalytic activity, obviously due to the electron-donating effect. A plausible reaction mechanism based on the related precedent studies is proposed (see Scheme S2, Supporting Information).[31] The C−H bond of alkyne is activated by Au active phases to form a nucleophilic gold acetylide. At the same time, the aldehyde is activated by a close SO_3H acid moiety in the Au-HS/SO_3H-PMO(Et) catalyst to facilely generate a requisite iminium ion, which is subjected to nucleophilic addition of the gold acetylide to lead to the effective one-pot A^3-coupling reaction.

Catalyst Recycling. The impressive results obtained led us to investigate the important issue of recyclability of the Au-SH/SO_3H-PMO(Et) catalyst. As shown Figure 8, the Au-SH/SO_3H-PMO(Et) catalyst could be easily recycled and subsequently reused up to 10 times in water-medium hydration of phenylacetylene, but the Au/SO_3H-PMO(Et) exhibited a rapid decrease in the catalytic efficiency in parallel studies. The ICP analysis revealed that the Au loading in the Au-SH/SO_3H-PMO(Et) decreased only by 4.0% after being reused 10 times (see Table 1), while the Au loading in the Au/SO_3H-PMO(Et) decreased by 16% after being reused 3 times, obviously due to the absence of coordination interaction between Au and SO_3H groups. Meanwhile, the TEM image (Figure S6, Supporting Information) revealed that the Au nanoparticles still kept high dispersion with average diameter less than 5 nm after being reused 10 times. Obviously, the coordination between Au nanoparticles and HS ligands could effectively inhibit both the leaching of Au from the support and the aggregation of Au nanoparticles. Furthermore, the N_2 adsorption−desorption isotherms (Figure S7, Supporting Information) and XRD patterns (Figure S8, Supporting Information) demonstrated that the Au-SH/SO_3H-PMO(Et) still remained an ordered mesoporous structure, corresponding to the high S_{BET}, V_P, and D_P (see Table 1), showing the excellent hydrothermal stability due to Et groups incorporated into the silica walls which could prevent the mesoporous structure from water-erosion. The slight decrease in the activity from 99% to 83% could be possibly attributed to the increase of Au nanoparticle size from 1−2 nm to 4−5 nm.

CONCLUSION

In conclusion, we have developed a novel Au-SH/SO_3H-PMO(Et) nanostructure with tiny Au nanoparticles and SO_3H acid groups terminally bonded to the ethyl-bridged PMO support, which acted as a bifunctional catalyst for alkyne hydration reactions in a cooperative manner. These reactions proceeded efficiently in aqueous media without using any organic solvents and even under solvent-free conditions. Such catalyst also exhibited high activity and selectivity in water-medium intramolecular hydroamination, styrene oxidation, and three-component coupling reactions. Moreover and importantly, the catalyst could be conveniently recycled and reused at least 10 times. These studies demonstrate the significant potential of its practical applications in organic synthesis. The strategy can be extended to immobilize other organometallics for catalysis.

EXPERIMENTAL SECTION

1. Catalyst Preparation. *(a). Au-HS/SO_3H-PMO(Et).* Thiol(HS)-functionalized ethyl-bridged PMO, denoted as HS-PMO(Et), was synthesized by self-assembly assisted co-condensation of bis-(triethoxysilyl)ethane (BTEE) and (3-mercaptopropyl) trimethoxysilane (MPTMS). First, triblockcopolymer P123 (1.0 g, [EO_{20}-PO_{70}-EO_{20}] M_{avg} = 5800) and KCl (3.0 g) were dissolved in 31 mL of 0.50 M HCl aqueous solution and stirred at 40 °C for 3 h. Then, 1.8 mL of BTEE was added and stirred for 1.5 h at 40 °C. Finally, MPTMS (0.13 mL) was added, and the reaction mixture was stirred for 24 h at 40 °C. The mixture was hydrothermally treated at 100 °C for 24 h. The solid was recovered by filtration and washed thoroughly with distilled water, followed by drying at 80 °C for 10 h under vacuum and extracting by refluxing the sample in 500 mL of ethanol solution at 80 °C for 24 h to remove surfactant and other organic residues.

A certain amount of HS-PMO(Et) was added into 7.0 mL of 0.017 M $HAuCl_4$ ethanol solution at room temperature for 24 h. After thoroughly washing with distilled water and ethanol, the powder was dried at 80 °C

under vacuum overnight. According to the ICP analysis, the Au loading in the Au-HS/SO_3H-PMO(Et) sample was determined as 0.10 mmol/g.

(b). Au-HS/SO_3H-SBA-15. P123 (1.0 g), KCl (3.0 g), and tetraethoxysilane (2.1 mL, TEOS) were mixed in 7.6 mL of H_2O and 15 mL of 2.0 M HCl aqueous solution. After being prehydrolyzed for 1.5 h at 40 °C, 0.13 mL of MPTMS was added into the solution, followed by stirring at 40 °C for 24 h and aging at 100 °C for 24 h. The precipitate was filtrated and dried at vacuum overnight. Then, the surfactants and other organic substances were extracted and washed away by refluxing the sample in ethanol solution at 80 °C for 24 h, followed by drying at 80 °C under vacuum overnight. The as-prepared SH-SBA-15 was then dispersed in 7.0 mL of 0.017 M $HAuCl_4$ ethanol solution at room temperature, followed by stirring for 24 h. After being thoroughly washed with distilled water and ethanol, the sample was dried at 80 °C under vacuum overnight. The ICP analysis showed that the Au loading in the as-prepared Au-HS/SO_3H-SBA-15 was 0.092 mmol/g.

(c). Preparation of Au/HS-PMO(Et). First, the Au nanoparticles were prepared according the following procedures. In a typical run of synthesis, 10 mL of tetralin, 10 mL of oleylamine, and $HAuCl_4 \cdot 3H_2O$ (0.10 g) were mixed at 40 °C and stirred under N_2 flow for 10 min, followed by adding a solution containing *tert*-butylamine-borane complex (0.50 mmol), 1.0 mL of tetralin, and 1.0 mL of oleylamine. After reaction at 40 °C for 1 h, 60 mL of acetone was added to settle down the precipitate, which was followed by washing thoroughly with acetone, leading to the Au nanoparticles with the average size around 3.0 nm. Then, the as-received Au nanoparticles were dispersed in hexane, followed by adding HS-PMO(Et) and stirring at 40 °C under N_2 flow for 4 h. The solid product was washed thoroughly with hexane and ethanol, followed by drying at 80 °C under vacuum overnight. The Au loading in the as-prepared Au-HS-PMO(Et) was determined as 0.12 mmol/g by ICP analysis.

(d). Au/SO_3H-PMO(Et). First, the SO_3H-PMO was synthesized by oxidizing the HS-PMO(Et) with H_2O_2 according to the following procedures. HS-PMO(Et) (0.30 g) was suspended in 10 g of aqueous solution containing 30 wt % H_2O_2. After being stirred at 40 °C for 24 h, the solid was filtered, washed with water and ethanol, and treated with 1.0 M H_2SO_4 solution for 2 h. The solid product was washed again with water and ethanol, followed by drying at 60 °C under vacuum overnight. Then, the Au/SO_3H-PMO(Et) was prepared according to the similar procedure used for preparing Au-HS-PMO(Et). The Au loading was determined as 0.10 mmol/g by ICP analysis.

2. Characterization. Fourier transform infrared (FT-IR) spectra were collected on a Nicolet Magna 550 spectrometer. X-ray powder diffraction (XRD) data were acquired on a SCINTAG PADX diffractometer using Cu Ka radiation. N_2 adsorption−desorption isotherms were measured at −196 °C on a Quantachrome NOVA 4000e analyzer, from which the specific surface area (S_{BET}), the pore volume (V_P), and the average pore diameter (D_P) were calculated by applying multiple-point Brunauer−Emmett−Teller (BET) and Barrett−Joyner−Halenda (BJH) models on adsorption branches, respectively. Surface morphology, porous structure, and Au particle size were observed through a transmission electron microscope (TEM, JEOL JEM2011). Solid NMR spectra were recorded on a Bruker DRX-400 NMR spectrometer. The UV−visible diffuse reflectance spectra (DRS) were performed on a MC-2530. Thermogravimetric analysis and differential thermal analysis (TG/DTA) were conducted on a DT-60. The surface electronic states were analyzed by X-ray photoelectron spectroscopy (XPS, Perkin-Elmer PHI 5000C ESCA). All the binding energy values are calibrated by using C_{1S} = 284.6 eV as a reference. The Au loading was determined by an inductively coupled plasma optical emission spectrometer (ICP-OES, Varian VISTA-MPX). Carbon monoxide chemisorption was conducted on a Micromeritics Autochem II instrument at ambient temperature (He/CO mixture with 10% of CO). X-ray absorption spectra at the Au L_3 edge of samples were collected in the fluorescence mode on the BL14W1 beamline of the Shanghai Synchrotron Radiation Facility (SSRF). A positron beam energy of 2.5 GeV and an average stored current of 250 mA were used. The photon energy range was 4000−12 500 eV with 1 × 1010 photons/s photon flux. A cryogenically cooled double-crystal Si(111) monochromator was used to minimize the presence of harmonics. The reference Au foil was used to calibrate the X-ray energy during each scan. The EXAFS spectra were analyzed by the NSRLXAFS 3.0 package according to standard procedures.[32]

3. Activity Test. *(a). Solvent-Free and Water-Medium Alkyne Hydration Reactions (Tables 1 and 2).* The solvent-free and water-medium alkyne hydrations were carried out in a 10 mL round-bottomed flask at a given temperature for a specified time. For solvent-free alkyne hydration, the reaction was carried out at 70 °C with a catalyst containing Au (0.010 mmol) and alkyne (0.25 mmol). For water-medium alkyne hydration, the reaction was carried out at 80 °C with a catalyst containing Au (0.010 mmol) and alkyne (0.25 mmol) and 4.0 mL of H_2O. After reaction for a desired time, the products were extracted by ethyl acetate, followed by analysis on a GC-17A gas chromatograph (SHIMADZU) equipped with a JWDB-5, 95% dimethyl-1-(5%)-diphenylpolysiloxane column and an FID detector. The column temperature was programmed from 80 to 250 °C at a speed of 10 °C/min. N_2 was used as the carrier gas, and *n*-decane was used as an internal standard.

(b). Water-Medium Intramolecular Hydroamination Reactions (Table 3). Water-medium intramolecular hydroamination reactions were conducted in a 10 mL round-bottomed flask in the presence of a catalyst containing Au (0.010 mmol), 1,5-hexadiyne (0.75 mmol), aniline (0.25 mmol), and 4.0 mL of H_2O at 80 °C for 24 h. The products were extracted with ethyl acetate and analyzed on a GC-17A gas chromatograph (SHIMADZU) equipped with a JWDB-5, 95% dimethyl 1-(5%)-diphenylpolysiloxane column and an FID detector. The column temperature was programmed from 80 to 250 °C at a speed of 10 °C/min. N_2 was used as carrier gas, and *n*-decane was used as an internal standard. The reaction conversion was calculated by aniline since 1,5-hexadiyne was in great excess.

(c). Water-Medium Styrene Oxidation (Table 3). Water-medium oxidation reactions were conducted in a similar way as described in the intramolecular hydroamination reaction: A mixture of a catalyst containing Au (0.020 mmol), styrene (1.0 mmol), anhydrous *t*-butyl hydroperoxide (1.5 mmol), and 4.0 mL of H_2O was heated at 82 °C for 24 h. The product analysis was also performed in the same procedure by using *n*-decane as an internal standard, as described for the intramolecular hydroamination reaction.

(d). Water-Medium A^3-Coupling Reactions (Table 4). Water-medium A^3-coupling reactions were conducted in a similar way as described in the intramolecular hydroamination reaction: A mixture of Au (0.015 mmol), benzaldehyde (0.25 mmol), phenylacetylene (0.30 mmol), piperidine (0.38 mmol), and 5.0 mL of water was heated at 70 °C for 12 h. The product analysis was also performed in the same procedure by using *n*-decane as an internal standard, and the reaction conversion was calculated based on the benzaldehyde.

4. Recycling Test. To determine the catalyst durability, the catalyst was allowed to centrifuge after each run of reactions, and the clear supernatant liquid was decanted slowly. The catalyst was washed thoroughly with distilled water and ethanol, followed by drying at 80 °C for 8 h under vacuum conditions. Then, the catalyst was reused with fresh charge of reactants for subsequent recycle under the identical reaction conditions.

■ ASSOCIATED CONTENT

Ⓢ Supporting Information. Schemes for the preparation of HS-PMO(Et) containing P123 templates and an A^3-coupling reaction mechanism and characterization spectra of the materials.

This material is available free of charge via the Internet at http://pubs.acs.org.

AUTHOR INFORMATION

Corresponding Author
wwang@unm.edu; hexing-li@shnu.edu.cn

ACKNOWLEDGMENT

This work was supported by the National Natural Science Foundation of China (20825724), the Project from Chinese Education Ministry (20070270001), and Shanghai local government (S30406 and 07dz22303).

REFERENCES

(1) (a) Jacobsen, E. N.; Pfaltz, A. *Comprehensive Asymmetric Catalysis I-III*; Springer: New York, 1999. (b) Crabtree, R. H. *The Organometallic Chemistry of the Transition Metals*; Wiley: New York, 2009.

(2) (a) Lindstrom, U. M. *Chem. Rev.* **2002**, *102*, 2751. (b) Li, C. J.; Chan, T. H. *Comprehensive Organic Reactions in Aqueous Media*, 2nd ed.; Wiley: New York, 2007.

(3) (a) Sheldon, R. A. *Green Chem.* **2005**, *7*, 267. (b) Metivier, P. *Fine Chemicals through Heterogeneous Catalysis*; Wiley: Weinheim, 2001.

(4) For recent reviews of gold catalysis, see: (a) Gagosz, F. *Tetrahedron* **2009**, *65*, 1757. (b) Gorin, D. J.; Sherry, B. D.; Toste, F. D. *Chem. Rev.* **2008**, *108*, 3351. (c) Arcadi, A. *Chem. Rev.* **2008**, *108*, 3266. (d) Widenhoefer, R. A. *Chem.—Eur. J.* **2008**, *14*, 5382. (e) Li, Z.; Brouwer, C.; He, C. *Chem. Rev.* **2008**, *108*, 3239. (f) Bongers, N.; Krause, N. *Angew. Chem., Int. Ed.* **2008**, *47*, 2178. (g) Ishida, T.; Haruta, M. *Angew. Chem., Int. Ed.* **2007**, *46*, 7154. (h) Hashmi, A.; Stephen, K. *Chem. Rev.* **2007**, *107*, 3180. (i) Zhang, L.; Sun, J.; Kozmin, S. A. *Adv. Synth. Catal.* **2006**, *348*, 2271.

(5) For a review on alkyne hydration, see: (a) Hintermann, L.; Labonne, A. *Synthesis* **2007**, 1121. For selected examples on Au-catalyzed alkyne hydration, see: (b) Norman, R. O. C.; Parr, W. J. E.; Thomas, C. B. *J. Chem. Soc., Perkin Trans. 1* **1976**, 1983. (c) Fukuda, Y.; Utimoto, K. *J. Org. Chem.* **1991**, *56*, 3729. (d) Casado, R.; Contel, M.; Laguna, M.; Romero, P.; Sanz, S. *J. Am. Chem. Soc.* **2003**, *125*, 11925. (e) Roembke, P.; Schmidbaur, H.; Cronje, S.; Raubenheimer, H. *J. Mol. Catal. A: Chem.* **2004**, *212*, 35. (f) Mizushima, E.; Sato, K.; Hayashi, T.; Tanaka, M. *Angew. Chem., Int. Ed.* **2002**, *41*, 4563. (g) Marion, N.; Ramón, R. S.; Nolan, S P. *J. Am. Chem. Soc.* **2009**, *131*, 448.

(6) For reviews, see: (a) Corma, A.; García, H. *Chem. Soc. Rev.* **2008**, *37*, 2096. (b) Chem, M.; Goodman, D. W. *Chem. Soc. Rev.* **2008**, *37*, 1860. (c) Hashmi, A. S. K.; Hutchings, G. J. *Angew. Chem., Int. Ed.* **2006**, *45*, 7896. (d) Haruta, M. *Chem. Rec.* **2003**, *3*, 75.

(7) Examples of Au-catalyzed cross-coupling reactions, see: (a) González-Arellano, C.; Abad, A.; Corma, A.; García, H.; Iglesias, M.; Sánchea, F. *Angew. Chem., Int. Ed.* **2007**, *46*, 1536. (b) Han, J.; Liu, Y.; Guo, R. *J. Am. Chem. Soc.* **2009**, *131*, 2060. (c) Kanuru, V. K.; Kyriakou, G.; Beaumont, S. K.; Papageorgiou, A. C.; Watson, D. J.; Lambert, R. M. *J. Am. Chem. Soc.* **2010**, *132*, 8081. (d) Beaumont, S. K.; Kyriakou, G.; Lambert, R. M. *J. Am. Chem. Soc.* **2010**, *132*, 12246. (e) Corma, A.; Juárez, R.; Boronat, M.; Sánchez, F.; Iglesias, M.; García, H. *Chem. Commun.* **2011**, *47*, 1446.

(8) Examples of Au(0)-catalyzed oxidations: (a) Haruta, M.; Kobayashi, T.; Sano, H.; Yamada, N. *Chem. Lett.* **1987**, 405. (b) Abad, A.; Concepción, P.; Corma, A.; García, H. *Angew. Chem., Int. Ed.* **2005**, *44*, 4066. (c) Mitsudome, T.; Noujima, A.; Mizugaki, T.; Jitsukawa, K.; Kaneda, K. *Green Chem.* **2009**, *11*, 793. (d) Polyene epoxidations: Choudhary, V. R.; Durnbre, D. K. *Catal. Commun.* **2009**, *10*, 1738. (e) Oxidation of alkanes: Chen, L.; Hu, J.; Richards, R. *J. Am. Chem. Soc.* **2009**, *131*, 914. (f) Reduction of nitro groups: Chen, Y.; Qiu, J.; Wang, X.; Xiu, J. *J. Catal.* **2006**, *242*, 227.

(9) (a) Haruta, M.; Yamada, N.; Kobayashi, T.; Iijima, S. *J. Catal.* **1989**, *115*, 301. (b) Chen, L. F.; Hu, J. C.; Richards, R. *J. Am. Chem. Soc.* **2009**, *131*, 914. (c) Haruta, M. *Catal. Today* **1997**, *36*, 153.

(10) Corti, C. W.; Holliday, R. J.; Thompson, D. T. *Appl. Catal A: Gen.* **2005**, *291*, 253.

(11) (a) Sayari, A.; Hamoudi, S. *Chem. Mater.* **2001**, *13*, 3151. (b) Fujita, S.; Inagaki, S. *Chem. Mater.* **2008**, *20*, 891. (c) Recently we have used PMO for the immobilization of transition metals for catalysis: Huang, J. L.; Zhu, F. X.; He, W. H.; Zhang, F.; Wang, W.; Li, H. X. *J. Am. Chem. Soc.* **2010**, *132*, 1492.

(12) Datta, K. K. R.; Reddy, B. V. S.; Ariga, K.; Vinu, A. *Angew. Chem., Int. Ed.* **2010**, *49*, 1.

(13) (a) Turner, M.; Golovko1, V. B.; Vaughan, O. P. H.; Abdulkin, P.; Berenguer-Murcia, A.; Tikhov, M. S.; Johnson, B. F. G.; Lambert, R. M. *Nature* **2008**, *454*, 981. (b) Ono, L. K.; Sudfeld, D.; Cuenya, B. R. *Surf. Sci.* **2006**, *600*, 5041.

(14) (a) Zhao, D. Y.; Huo, Q. S.; Feng, J. L.; Chmelka, B. F.; Stucky, G. D. *J. Am. Chem. Soc.* **1998**, *120*, 6024. (b) Zhu, H. G.; Jones, D. J.; Zajac, J.; Dutartre, R.; Rhomari, M.; Rozière, J. *Chem. Mater.* **2002**, *14*, 4886. (c) Burleigh, M.; Michael, A.; Markowitz, M.; Spector, S.; Gaber, B. *J. Phys. Chem. B* **2001**, *105*, 9935.

(15) (a) Krcher, O.; Kppel, R. A.; Frba, M. *J. Catal.* **1998**, *178*, 284. (b) Hu, Q. Y.; Hampsey, J. E.; Jiang, N.; Li, C. J.; Lu, Y. F. *Chem. Mater.* **2005**, *17*, 1561.

(16) (a) Lagadic, L.; Mitchell, M. K.; Payne, B. D. *Environ. Sci. Technol.* **2001**, *35*, 984. (b) Wang, X. G.; Cheng, S.; Chan, J. C. C. *J. Phys. Chem. C* **2007**, *111*, 2156.

(17) (a) Jiang, D. M.; Gao, J. S.; Yang, Q. H.; Yang, J.; Li, C. *Chem. Mater.* **2006**, *18*, 6012. (b) Inagaki, S.; Guan, S.; Fukushima, Y.; Terasak, O. *J. Am. Chem. Soc.* **1999**, *121*, 9611.

(18) (a) Wua, H. Y.; Liao, C. H.; Pan, Y. C.; Yeh, C. L.; Kao, H. M. *Microporous Mesoporous Mater.* **2009**, *119*, 109. (b) Jones, J. T. A.; Wood, C. D.; Dickinson, C.; Khimyak, Y. Z. *Chem. Mater.* **2008**, *20*, 3385. (c) Mohanty, P.; Linn, N. M. K.; Landskron, K. *Langmuir* **2010**, *26*, 1147.

(19) Margolese, D.; Melero, J. A.; Christiansen, S. C.; Chmelka, B. F.; Stucky, G. D. *Chem. Mater.* **2000**, *12*, 2448.

(20) (a) Yang, L. M.; Wang, Y. J.; Luo, G. S.; Dai, Y. Y. *Microporous Mesoporous Mater.* **2005**, *84*, 275. (b) Yang, Q.; Kapoor, M. P.; Inagaki, S. *J. Am. Chem. Soc.* **2002**, *124*, 9694. (c) Kapoor, M. P.; Yang, Q.; Goto, Y.; Inagaki, S. *Chem. Lett.* **2003**, *32*, 914.

(21) Kang, T.; Park, Y.; Yi, J. *Ind. Eng. Chem. Res.* **2004**, *43*, 1478.

(22) Beck, J.; Vartuli, J.; Roth, W. *J. Am. Chem. Soc.* **1992**, *114*, 10834.

(23) Matos, J. R.; Kruk, M.; Mercuri, L. P.; Jaroniec, M.; Asefa, T.; Coombs, N.; Ozin, G. A.; Kamiyama, T.; Terasaki, J. *Chem. Mater.* **2002**, *14*, 1903.

(24) Whyte, T. E., Jr. *Catal. Rev.* **1974**, *8*, 117.

(25) (a) Yao, T.; Sun, Z. H.; Li, Y. Y.; Pan, Z. Y.; Wei, H.; Xie, Y.; Nomura, M.; Niwa, Y.; Yan, W. S.; Wu, Z. Y.; Jiang, Y.; Liu, Q. H.; Wei, S. Q. *J. Am. Chem. Soc.* **2010**, *132*, 7696. (b) Zhang, P.; Zhou, X.; Tang, Y. H.; Sham, T. K. *Langmuir* **2005**, *21*, 8502.

(26) Miller, J. T.; Kropf, A. J.; Zha, Y.; Regalbuto, J. R.; Delannoy, L.; Louis, C.; Bus, E.; Bokhoven, J. A. v. *J. Catal.* **2006**, *240*, 222.

(27) (a) Li, H. X.; Chen, J.; Wan, Y.; Zhang, F.; Lu, Y. F. *Green Chem.* **2007**, *9*, 273. (b) Wan, Y.; Chen, J.; Zhang, D. Q.; Li, H. X. *J. Mol. Catal. A* **2006**, *258*, 89.

(28) Zhang, Y. H.; Donahue, J. P.; Li, C. J. *Org. Lett.* **2007**, *9*, 627.

(29) Xing, D.; Guan, B.; Cai, G.; Fang, Z.; Yang, L.; Shi, Z. *Org. Lett.* **2006**, *8*, 693.

(30) Wei, C.-M.; Li., C.-J. *J. Am. Chem. Soc.* **2003**, *125*, 9584.

(31) (a) Kidwai, M.; Bansal, V.; Kumar, A.; Mozumdar, S. *Green Chem.* **2007**, *9*, 742. (b) Sreedhar, B.; Kumar, A. S.; Reddy, P. S. *Tetrahedron Lett.* **2010**, *51*, 1891.

(32) Lengeler, B.; Eisenberger, P. *Phys. Rev. B* **1980**, *21*, 4507.